Available online at www.sciencedirect.com
SCIENCE DIRECT®
International Journal of Heat and Mass Transfer 47 (2004) 3017–3030
International Journal of HEAT and MASS TRANSFER
www.elsevier.com/locate/ijhmt

Cavity flow in a porous medium driven by differential heating

P.G. Daniels *, M. Punpocha [1]

Centre for Mathematical Science, City University, Northampton Square, London, EC1V 0HB, UK

Received 28 March 2003; received in revised form 3 March 2004

Abstract

This paper describes flow through a porous medium in a two-dimensional cavity driven by differential heating of the upper surface. The lower surface and sidewalls of the cavity are thermally insulated and the main emphasis is on the case where the temperature distribution at the upper surface is monotonic, resulting in a single-cell circulation. Numerical results for general values of the Darcy–Rayleigh number R and the cavity aspect ratio L are compared with theoretical predictions for the small Darcy–Rayleigh number limit ($R \to 0$) where the temperature field is conduction-dominated, and an approximate theory for the large Darcy–Rayleigh number limit ($R \to \infty$) where convection is significant. In the latter case a horizontal boundary-layer structure is identified near the upper surface. This conveys fluid to the cold end of the cavity where it descends in a narrow vertical jet in the corner. The temperature is almost constant throughout the remainder of the cavity, and heat transfer arguments and boundary-layer theory are used to predict its value.

1. Introduction

Porous media play an important role in many topical areas of application including geothermal energy systems, oil and gas recovery, the spread of pollution in groundwater and cavity wall insulation. Previous studies of thermal convection in porous media can be divided into two main groups, those where the heating is from below and flow is generated typically by an instability mechanism of the type first discussed by Lapwood [1] and those where the heating is from the side and horizontal thermal gradients generate motion. In the latter case, most previous studies have been concerned with the case of a two-dimensional cavity where the vertical walls of the cavity are maintained at different constant temperatures. For a porous medium governed by Darcy's law there are two main parameters, the aspect ratio L of the cavity (width/depth) and the Darcy–Rayleigh number R which is a non-dimensional measure of buoyancy forces relative to frictional forces (see (4)).

For the side-heated cavity, extensive numerical solutions have been reported in [2–4], and experimental investigations have also been carried out [5–8]. Weber[9] considered the large Darcy–Rayleigh number structure ($R \to \infty$ at fixed L) for the side heated cavity with insulated upper and lower surfaces, demonstrating the existence of vertical boundary layers of thickness $O(R^{-1/2})$, whilst Walker and Homsy [10] considered the flow properties for large aspect ratio L and in the large and small R limits for fixed L. Blythe, Daniels and Simpkins [11] considered the structure of the vertical boundary layers near the corners in the large R limit enabling subsequently a double horizontal boundary-layer structure, consisting of layers of thickness $O(R^{-1/4})$ and $O(R^{-5/16})$ to be identified [12]. Further asymptotic structures in side-heated shallow and tall cavities have been discussed in [13–16].

Other related work involving horizontal thermal gradients includes the horizontal boundary-layer analysis of Cheng and Chang [17] and Chang and Cheng [18] who considered similarity solutions of the boundary-layer equations on a heated horizontal wall, and the stability of porous media flows on horizontal surfaces has been considered by Rees and Bassom [19,20]. Porous media boundary-layer flows on heated vertical surfaces have been studied in [21–25] and flows driven by thermal gradients in corner regions in [26–28]. Further examples and references are given by Nield and Bejan [29].

* Corresponding author.
[1] Present address: Department of Mathematics, King Mongkut's Institute of Technology, Bangkok 10800, Thailand.

0017-9310/$ - see front matter © 2004 Elsevier Ltd. All rights reserved.
doi:10.1016/j.ijheatmasstransfer.2004.03.004

Nomenclature

d	cavity width
g	acceleration due to gravity
h	cavity height
K	permeability
L	cavity aspect ratio
Q	heat flux
R	Darcy–Rayleigh number
S	non-dimensional temperature profile
T	non-dimensional temperature
T^*	temperature
ΔT	temperature differential
u, w	non-dimensional velocity components
x, z	non-dimensional coordinates
x^*, z^*	coordinates

Greek symbols

β	coefficient of thermal expansion
κ	thermal diffusivity
ν	kinematic viscosity
ψ	non-dimensional stream function

In the present work it is proposed to investigate thermally-driven flow in a two-dimensional cavity where the motion is driven by a temperature differential along the upper surface and the other walls are thermally insulated. Such flows are relevant in groundwater systems where there is uneven heating of the Earth's surface and in flows driven by localized heat sources such as the magma chamber of a caldera [30]. The mathematical problem is formulated in Section 2, with attention focused on the case of a monotonic temperature distribution along the upper surface. For small Darcy–Rayleigh numbers the single-cell circulation is conduction-dominated and in Section 3 the main features of the solution are obtained for general aspect ratios L using a perturbation analysis. Results for general Darcy–Rayleigh numbers up to $R = 5000$ are obtained using an explicit finite difference scheme and are described in Section 4. Major emphasis is placed on the case of the square cavity ($L = 1$) although results are also obtained for other aspect ratios in the range $1/4 \leqslant L \leqslant 4$. One of the main purposes of the numerical work is to reveal the asymptotic structure of the solution that emerges as $R \to \infty$. In this limit it is found that the main features of the flow and temperature fields occur in a horizontal boundary layer near the upper surface and a vertical boundary layer near the top of the sidewall at the colder end. In Section 5 an approximate analytical solution for the horizontal boundary layer is obtained by neglecting the interaction with the vertical boundary layer. By considering the heat flux through the upper surface of the cavity, a prediction is obtained for the temperature in the core region of the cavity, below the horizontal boundary layer. The results are discussed in Section 6.

2. Formulation

A two-dimensional rectangular cavity $0 \leqslant x^* \leqslant d$, $0 \leqslant z^* \leqslant h$ is filled with a fluid-saturated porous medium. The upper boundary $z^* = h$ is held at temperature

$$T^* = T_0^* + \Delta T\, S(x^*/d), \tag{1}$$

where the function $S(x^*/d)$ varies monotonically from zero at $x^* = 0$ to 1 at $x^* = d$. The vertical walls $x^* = 0$ and $x^* = d$ and the bottom wall $z^* = 0$ are thermally insulated. Subject to Darcy's law and the Oberbeck-Boussinesq approximation, steady two-dimensional motion is governed by the non-dimensional equations

$$\nabla^2 \psi = -R \frac{\partial T}{\partial x}, \tag{2}$$

$$\nabla^2 T = \frac{\partial(T, \psi)}{\partial(x, z)}, \tag{3}$$

where $\psi(x, z)$ is the stream function non-dimensionalized by the thermal diffusivity κ, $T(x, z)$ is the temperature measured relative to T_0^* and non-dimensionalized by ΔT, (x, z) are Cartesian coordinates non-dimensionalized by h and R is the Darcy–Rayleigh number defined by

$$R = Kg\beta\Delta T h/\kappa\nu, \tag{4}$$

where K is the permeability, β is the coefficient of thermal expansion, ν is the kinematic viscosity and g is the acceleration due to gravity. The non-dimensional velocity components in the x, z directions are given by

$$u = \frac{\partial \psi}{\partial z}, \quad w = -\frac{\partial \psi}{\partial x}, \tag{5}$$

respectively.

The cavity walls are assumed to be impermeable, and so the relevant boundary conditions are

$$\psi = \frac{\partial T}{\partial x} = 0 \quad \text{on } x = 0, L, \tag{6}$$

$$\psi = \frac{\partial T}{\partial z} = 0 \quad \text{on } z = 0 \tag{7}$$

and

$$\psi = 0, \quad T = S(x/L) \quad \text{on } z = 1. \tag{8}$$

Solutions of the mathematical problem defined by (2), (3) and (6)–(8) depend on the Darcy–Rayleigh number R and the aspect ratio $L = d/h$, and also on the specific form of the temperature profile $S(x/L)$ at the upper surface.

3. Solution for small Darcy–Rayleigh numbers

In this section the temperature profile $S(x/L)$ is taken to have the simple form

$$S(x/L) = \frac{1}{2}(1 - \cos(\pi x/L)), \quad 0 \leqslant x \leqslant L, \tag{9}$$

so that the temperature T along the upper surface is antisymmetric about the mean value $\frac{1}{2}$ at $x = L/2$. The solution for small Darcy–Rayleigh numbers is obtained by assuming a perturbation expansion in powers of R:

$$T(x,z) = T_0(x,z) + RT_1(x,z) + \cdots, \tag{10}$$

$$\psi(x,z) = R\psi_1(x,z) + R^2\psi_2(x,z) + \cdots \tag{11}$$

Substitution into (3) shows that at leading order the temperature field T_0 is governed by Laplace's equation

$$\frac{\partial^2 T_0}{\partial x^2} + \frac{\partial^2 T_0}{\partial z^2} = 0, \tag{12}$$

which must be solved subject to

$$\frac{\partial T_0}{\partial x} = 0 \quad \text{on } x = 0, L, \tag{13}$$

$$\frac{\partial T_0}{\partial z} = 0 \quad \text{on } z = 0, \quad T_0 = S(x/L) \quad \text{on } z = 1. \tag{14}$$

The solution is thus dominated by conduction and is readily found to be

$$T_0 = \frac{1}{2}(1 - \operatorname{sech}(\pi/L)\cos(\pi x/L)\cosh(\pi z/L)). \tag{15}$$

From terms of order R in (2), the leading term ψ_1 in the stream function satisfies Poisson's equation

$$\frac{\partial^2 \psi_1}{\partial x^2} + \frac{\partial^2 \psi_1}{\partial z^2} = -\frac{\partial T_0}{\partial x}, \tag{16}$$

which must be solved subject to $\psi_1 = 0$ on the boundaries. The solution is found to be

$$\psi_1 = \frac{1}{4}(1 - z)\operatorname{sech}(\pi/L)\sinh(\pi z/L)\sin(\pi x/L). \tag{17}$$

The leading order terms $T_0 - \frac{1}{2}$ and ψ_1 are seen to be odd and even functions of $x - \frac{1}{2}L$, respectively, and their contours are shown in Fig. 1 for the case $L = 1$. The conductive temperature field drives a single-cell circulation with upward motion on the hotter side and downward motion on the colder side. The maximum value of the leading order stream function, which defines the centre of circulation, is $\psi_1 = 0.0288277$ and occurs at $x = \frac{1}{2}L$, $z = 0.689924$.

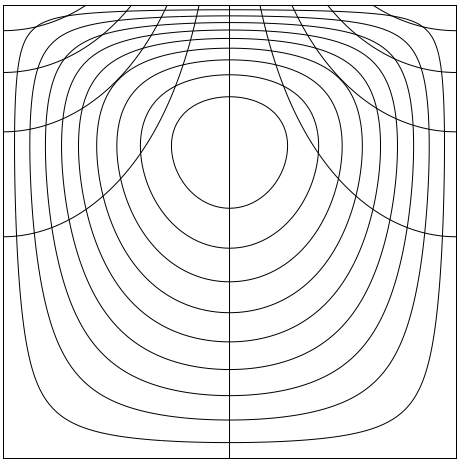

Fig. 1. Contours of T_0 and ψ_1 for the case $L = 1$.

From Eq. (3), equating coefficients of R shows that the first-order temperature field T_1 satisfies Poisson's equation

$$\frac{\partial^2 T_1}{\partial x^2} + \frac{\partial^2 T_1}{\partial z^2} = \frac{\partial T_0}{\partial x}\frac{\partial \psi_1}{\partial z} - \frac{\partial T_0}{\partial z}\frac{\partial \psi_1}{\partial x}, \tag{18}$$

which must be solved subject to

$$\frac{\partial T_1}{\partial x} = 0 \quad \text{on } x = 0, L, \tag{19}$$

$$\frac{\partial T_1}{\partial z} = 0 \quad \text{on } z = 0, \quad T_1 = 0 \quad \text{on } z = 1. \tag{20}$$

The solution is

$$\begin{aligned} T_1 = \frac{1}{256}\operatorname{sech}^2(\pi/L)\Big\{ & 4(1-z)\cosh(2\pi z/L) \\ & + \frac{2L}{\pi}(\sinh(2\pi z/L) - \sinh(2\pi/L)) \\ & + \Big(2\gamma\cosh(2\pi z/L) - \frac{L}{\pi}\mathrm{e}^{-2\pi z/L} \\ & + 2(z\cosh(2\pi z/L) + 2(1-z))\Big)\cos(2\pi x/L)\Big\}, \end{aligned} \tag{21}$$

where

$$\gamma = \frac{L}{\pi}(1 + \mathrm{e}^{4\pi/L})^{-1} - 1. \tag{22}$$

From Eq. (2), equating coefficients of R^2 shows that ψ_2 satisfies Poisson's equation

$$\frac{\partial^2 \psi_2}{\partial x^2} + \frac{\partial^2 \psi_2}{\partial z^2} = -\frac{\partial T_1}{\partial x}, \tag{23}$$

to be solved subject to $\psi_2 = 0$ on the boundaries. The solution is

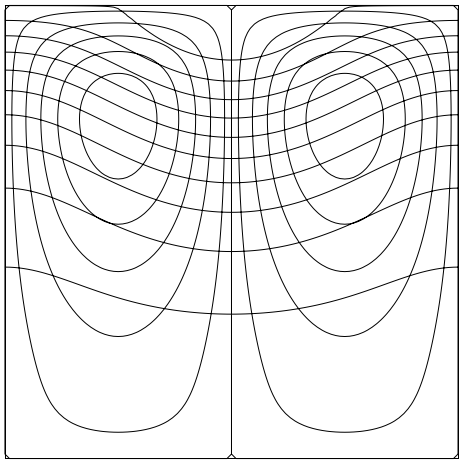

Fig. 2. Contours of T_1 and ψ_2 for the case $L = 1$.

$$\psi_2 = \frac{1}{256}\operatorname{sech}^2(\pi/L)\left\{\frac{1}{2}z^2\sinh(2\pi z/L) + z\mathrm{e}^{2\pi z/L}\left(\frac{\gamma}{2} - \frac{L}{8\pi}\right) + z\mathrm{e}^{-2\pi z/L}\left(\frac{3L}{8\pi} - \frac{\gamma}{2}\right) + \frac{2L}{\pi}(z - 1 + \cosh(2\pi z/L)) - \delta\sinh(2\pi z/L)\right\}\sin(2\pi x/L), \tag{24}$$

where

$$\delta = \frac{2L}{\pi}\coth(2\pi/L) + \left(\left(\frac{\gamma}{2} + \frac{1}{4} - \frac{L}{8\pi}\right)\mathrm{e}^{2\pi/L} + \left(\frac{3L}{8\pi} - \frac{\gamma}{2} - \frac{1}{4}\right)\mathrm{e}^{-2\pi/L}\right)\operatorname{cosech}(2\pi/L). \tag{25}$$

Contours of T_1 and ψ_2, which are even and odd functions of $x - \frac{1}{2}L$, respectively, are shown in Fig. 2 for the case $L = 1$. Although the leading order velocity and temperature fields have symmetry about the centreline $x = \frac{1}{2}L$ of the cavity, the correction terms (24) and (21) destroy this symmetry, as can be seen from contour plots of the overall temperature and stream function (10) and (11) for $R = 5$ and $R = 20$ in Fig. 3. As the Darcy–Rayleigh number increases, the centre of circulation shifts towards the upper cold corner, while the isotherms move around towards the hotter side.

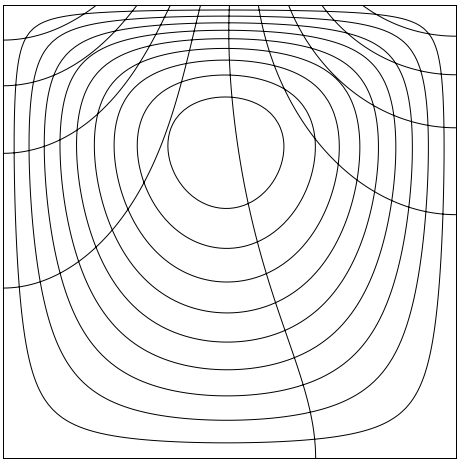

R = 5

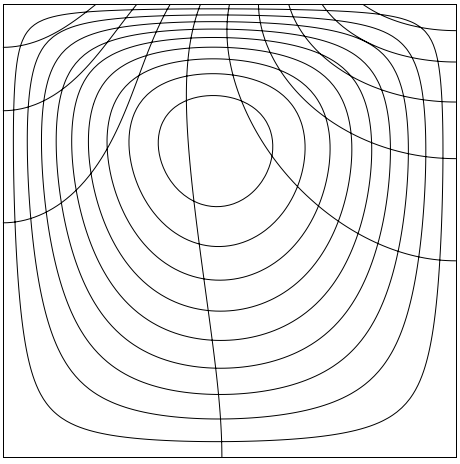

R = 20

Fig. 3. Isotherms and streamlines given by the two-term small Darcy–Rayleigh number approximation for $R = 5$ and $R = 20$ with $L = 1$.

4. Numerical solution for general Darcy–Rayleigh numbers

The steady-state system (2), (3) and (6)–(8) is elliptic but a simple method of finding solutions is to introduce artificial time derivatives

$$\frac{\partial\psi}{\partial t} = \nabla^2\psi + R\frac{\partial T}{\partial x}, \tag{26}$$

$$\frac{\partial T}{\partial t} = \nabla^2 T - \frac{\partial(T,\psi)}{\partial(x,z)} \tag{27}$$

to obtain a system which is parabolic in time. This allows a numerical solution to be found by a straightforward marching procedure in time, with the required steady-state results obtained in the limit of large time. An explicit forward difference method was used to solve (26),(27) and (6)–(8) together with an initial condition which was usually taken as $T = \psi = 0$ at $t = 0$. The equations were discretized on a uniform grid using standard second-order accurate central difference approximations for the spatial derivatives in the equations and forward differences for the time derivatives. In discretizing the boundary conditions for $\partial T/\partial x$ and

$\partial T/\partial z$ second-order accuracy was maintained by using a quadratic interpolation to evaluate T on the boundaries. The time step was chosen small enough to ensure numerical stability. Various checks were carried out with different spatial grid sizes to test the accuracy and temporal convergence of the scheme, and most of the results described here were obtained with step sizes of 0.01 in x and z and a time step of 10^{-5}. Typically convergence of the solution to its steady-state form occurred within a time $t = 2$ although this decreased with increasing Darcy–Rayleigh number. As an additional check on accuracy, the total heat flux at the upper boundary

$$Q = \int_0^L \frac{\partial T}{\partial z}(z = 1)\,\mathrm{d}x \tag{28}$$

was monitored using the trapezium rule with the value of $\partial T/\partial z$ calculated from a quadratic interpolation of T. Since the three lower walls are thermally insulated it follows from (3) that Q should be zero for the steady-state solution; in practice for $L = 1$ its steady-state value rose from 0.0027 at $R = 20$ to 0.041 at $R = 500$, representing relative errors of 0.14% and 0.7%, respectively, compared with the maximum steady-state value of $\partial T/\partial z$ on the upper surface.

4.1. Results for a cosine temperature profile

Initially results were obtained for $L = 1$ with the cosine profile (9) on the upper surface. Fig. 4 shows results for $R = 20, 200, 1500$ and 5000. For $R = 20$, the streamlines and isotherm patterns are in excellent agreement with the two-term analytical prediction shown in Fig. 3. As R increases, the centre of circulation moves towards the cold end of the upper boundary and the main

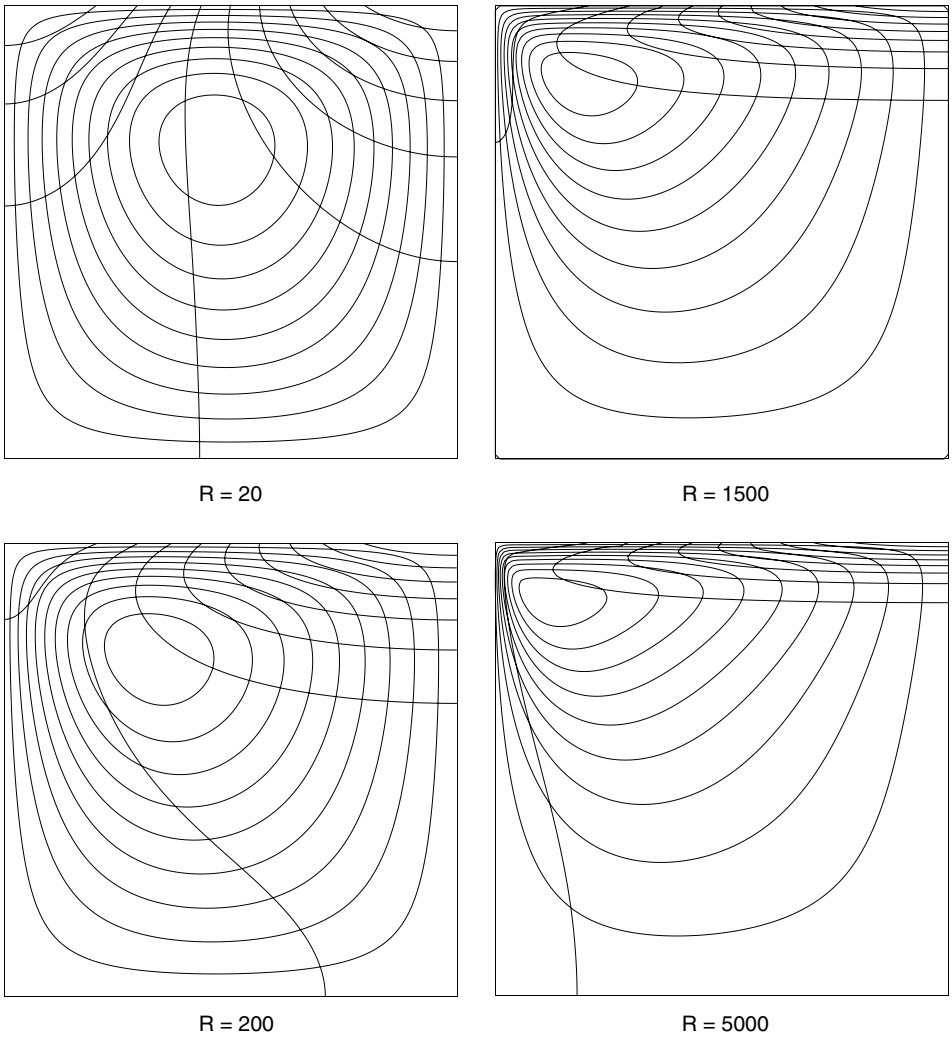

Fig. 4. Isotherms and streamlines of the steady-state numerical solution for the cosine profile with $R = 20, 200, 1500, 5000$ and $L = 1$.

temperature variation occurs near the upper surface. Fig. 5 shows the slip velocities on the four walls and indicates maximum flow speeds along the upper surface and at the top of the vertical wall on the cold side at large R. The local heat transfer through the upper surface is shown in Fig. 6; heat enters the cavity through the hotter part of

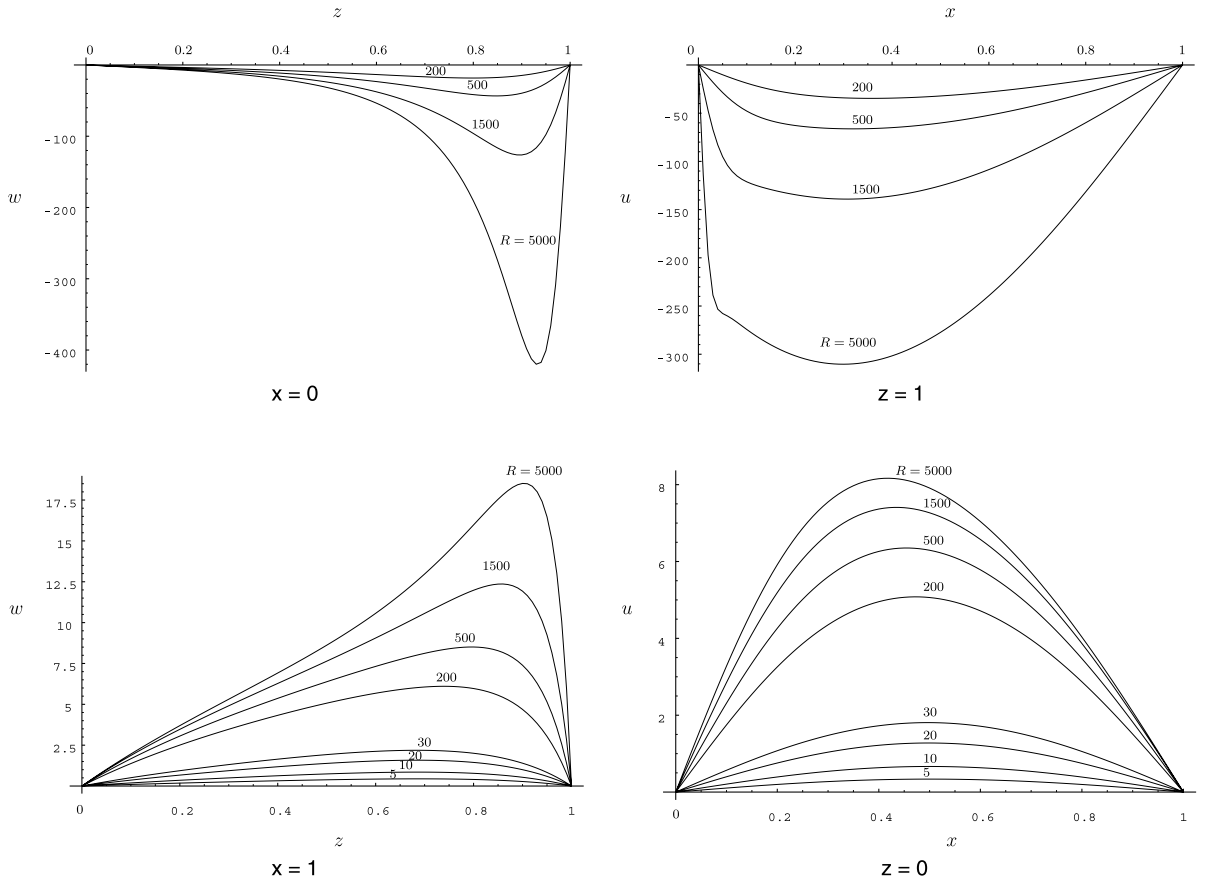

Fig. 5. Slip velocities on the four walls of the cavity at various values of R from the steady-state numerical solution for the cosine profile with $L = 1$.

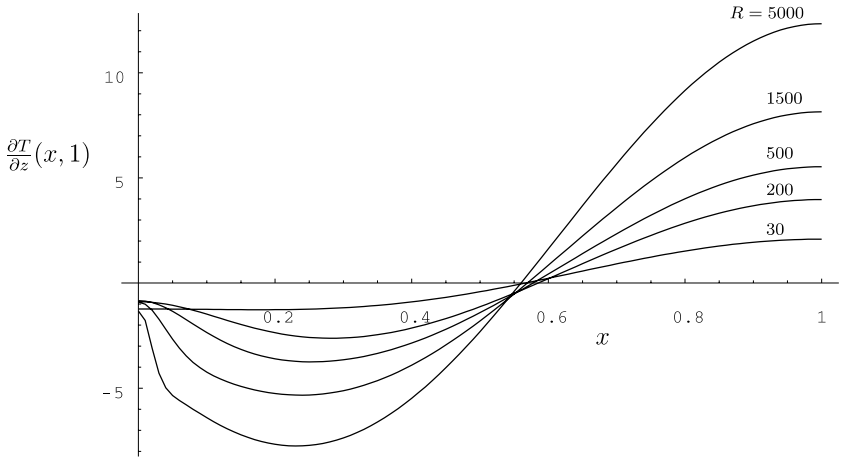

Fig. 6. Local heat transfer through the upper surface of the cavity for various values of R from the steady-state numerical solution for the cosine profile with $L = 1$.

the upper surface and leaves through the colder part, causing the fluid to lose buoyancy and descend rapidly in a narrow region near the vertical wall at large R; it then returns to the neighbourhood of the upper surface via a relatively slow circulation in the remainder of the cavity. The temperature in this region below the main thermal variation becomes almost constant as R increases, but does not approach the minimum temperature of the upper surface. Instead, it appears to approach a finite non-zero value of approximately 0.1, that is a temperature in excess of the minimum temperature by about 10 percent of the temperature difference imposed at the upper surface.

4.2. Results for a quadratic temperature profile

Results were also obtained for the quadratic temperature profile

$$S(x/L) = 1 - \left(1 - \frac{x}{L}\right)^2 \tag{29}$$

at the upper surface. Again this is monotonic in x and is studied partly because it allows an exact solution of the horizontal boundary-layer equations in the high Darcy–Rayleigh number limit, to be discussed in Section 5. This profile is also of interest in that unlike the cosine profile it is linear as it approaches the cold end $(x = 0)$, implying a more sudden drop in temperature there and thus a more vigorous motion. Mathematically, it also implies a weak singularity in the thermal field in the corner $(x = 0, z = 1)$ because the value of $\partial T/\partial x$ must adjust from $2L^{-1}$ given by (29) on $z = 1$ as $x \to 0+$ to zero on the vertical wall $x = 0$.

The behaviour of the solution is qualitatively similar to that for the cosine profile. At small values of R a series expansion (10) and (11) is again valid but now the leading terms

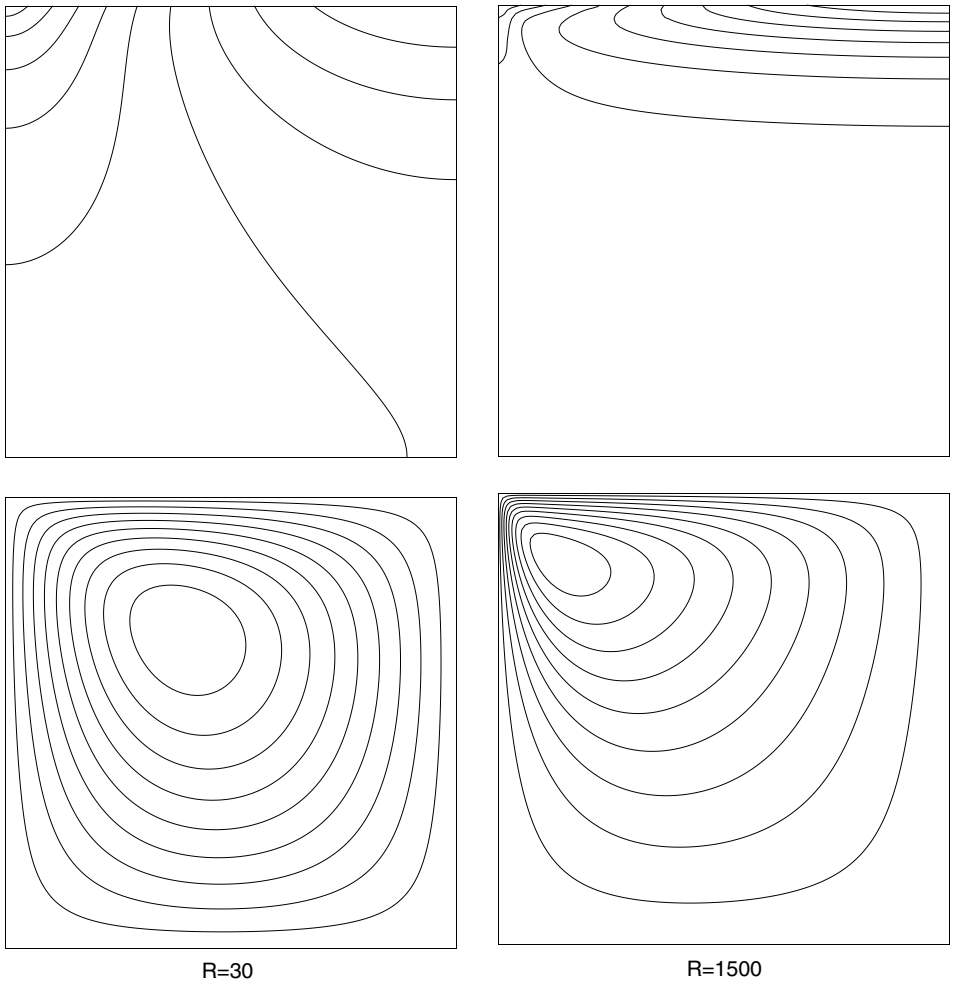

Fig. 7. Isotherms and streamlines of the steady-state numerical solution for the quadratic profile with $R = 30$, 1500 and $L = 1$.

$$T_0 = \frac{2}{3} + \sum_{n=1}^{\infty} C_n \cos(n\pi x/L)\cosh(n\pi z/L), \tag{30}$$

$$\psi_1 = \frac{1}{2}(z-1)\sum_{n=1}^{\infty} C_n \sin(n\pi x/L)\sinh(n\pi z/L), \tag{31}$$

where

$$C_n = -\frac{4}{(n\pi)^2}\operatorname{sech}(n\pi/L), \tag{32}$$

do not possess symmetry about $x = \frac{1}{2}L$. The centre of the single-cell circulation where ψ_1 attains its maximum value of 0.02342 is at $x = 0.44$, $z = 0.69$ when $L = 1$ and is thus closer to the cold end of the cavity than in the previous case. Fig. 7 shows steady-state isotherms and streamlines obtained from the numerical scheme for a square cavity at $R = 30$ and $R = 1500$. At large R, the overall structure of the solution is similar to that of the previous case although the eddy is centred a little closer to the corner; below the main thermal variation at the upper surface the almost constant temperature in the cavity is significantly higher than before, at a level in excess of the minimum temperature by about 23–24% of the temperature difference along the upper surface.

Results were also computed for aspect ratios L of $\frac{1}{4}$, $\frac{1}{2}$, 2 and 4. The same general features are observed, although for tall cavities (Fig. 8) the fact that the motion is being driven from the upper surface is evident for all values of R, with the centre of circulation always near the upper boundary. For $L = \frac{1}{4}$ and $R = 5000$, the temperature below the thermal layer at the upper surface is found to be around 0.279, whilst for the same Darcy–Rayleigh number and $L = \frac{1}{2}$, this near constant value is about 0.251.

For shallow cavities (Fig. 9) the bottom boundary has much more impact on the solution at general values of R although for $L = 4$ the development of the thermal layer at the upper surface is eventually evident when R exceeds 1500. At $R = 5000$ the temperature along the lower surface varies from 0.207 at $x = 0$ to 0.236 at $x = 4$. For small values of R and large values of L the isotherms align almost vertically in the middle section of the cavity and the streamlines are approximately symmetrical about $z = \frac{1}{2}$. This reflects the fact that the z derivatives on the left-hand sides of (2) and (3) dominate the x derivatives in this limit, and the relevant solution throughout most of the cavity $(0 < x/L < 1,\ 0 \leqslant z \leqslant 1)$ for $L \gg 1$ is

$$T \sim 1 - \left(1 - \frac{x}{L}\right)^2, \quad \psi \sim Rz(1-z)\left(1 - \frac{x}{L}\right). \tag{33}$$

An inner solution near $x/L = 0$ is necessary to allow ψ to adjust to zero at the cold end wall, but the details are not described here.

From the results presented here for general Darcy–Rayleigh numbers and various aspect ratios, it is clear

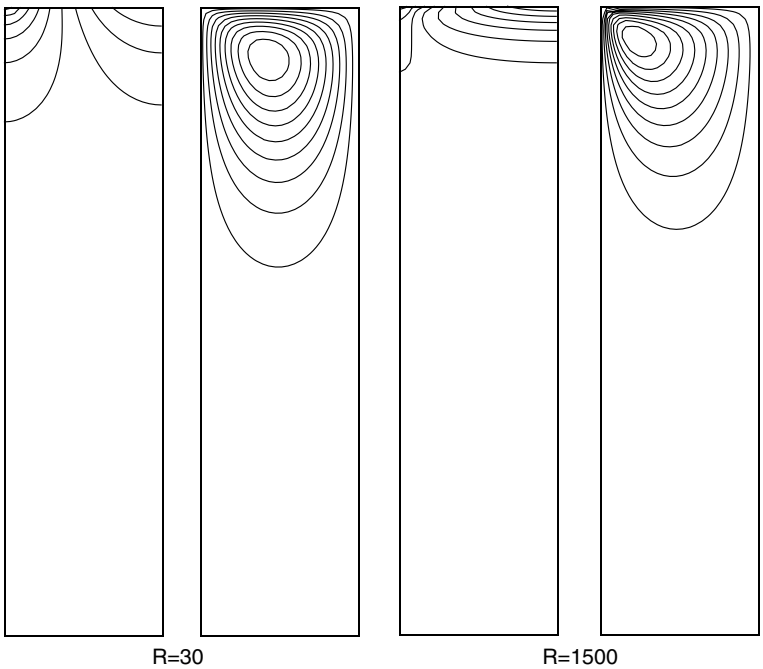

Fig. 8. Isotherms and streamlines of the steady-state numerical solution for the quadratic profile with $R = 30, 1500$ and $L = \frac{1}{4}$.

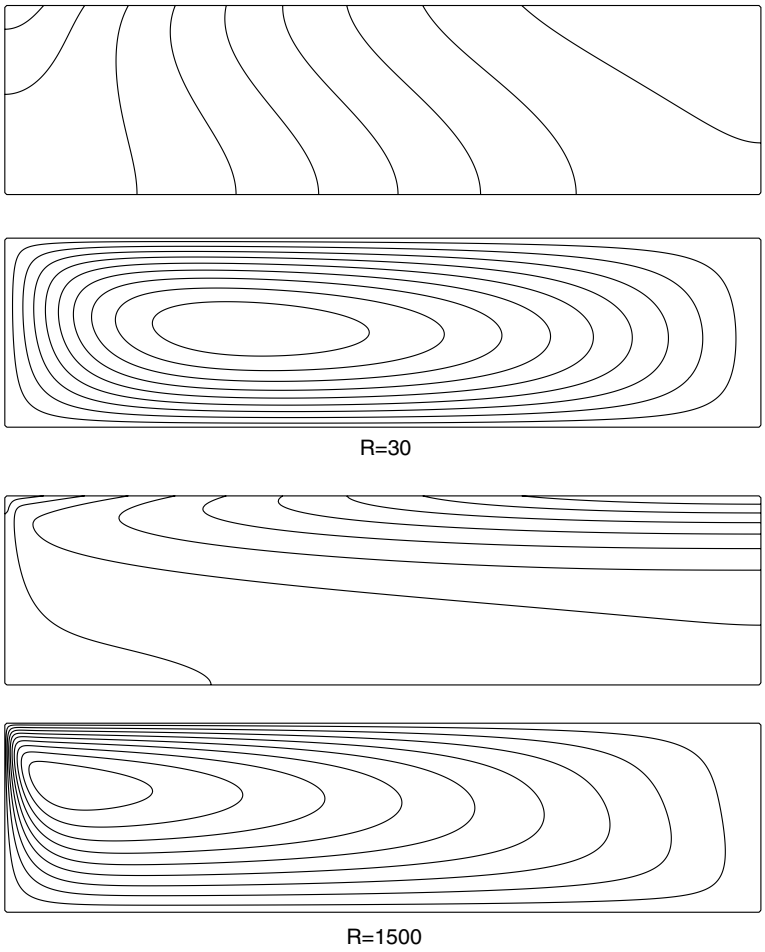

Fig. 9. Isotherms and streamlines of the steady-state numerical solution for the quadratic profile with $R = 30, 1500$ and $L = 4$.

that the solutions possess the same general features as R increases, with the formation of a horizontal boundary layer along the upper surface where the main temperature adjustment occurs, leaving the bottom part of the cavity with an almost constant temperature in the limit of large R. For the quadratic profile this temperature is in the range 0.2–0.3, with the precise value only weakly dependent on the aspect ratio L. For the cosine profile, the value is closer to 0.1. The main feature of the flow pattern is the migration of the centre of circulation towards the upper end of the colder sidewall as R increases, with a jet-like motion forming locally there in the limit of large R.

Table 1 gives values of both the temperature and stream function at the centre of the cavity as functions of R for the case $L = 1$. It also shows the behaviour of the maximum value of the stream function. Whereas $\psi(\frac{1}{2},\frac{1}{2})$ and $T(\frac{1}{2},\frac{1}{2})$ appear to approach finite limiting values as $R \to \infty$, the maximum stream function value is found to be an increasing function of R.

Table 1
Properties of the numerical solution for a square cavity with a quadratic temperature profile at the upper surface

R	$T(\frac{1}{2},\frac{1}{2})$	$\psi(\frac{1}{2},\frac{1}{2})$	$\psi_{\max}$	$\frac{\ln \psi_{\max}}{\ln R}$
5	0.6567	0.1006	0.1179	−1.3284
30	0.5916	0.5845	0.6997	−0.1050
200	0.3942	2.0341	3.0291	0.2092
500	0.3102	2.7641	5.0323	0.2600
1500	0.2517	3.4950	8.4403	0.2917
5000	0.2369	4.0844	13.8602	0.3087

5. An approximate theory for large Darcy–Rayleigh numbers

In this section an approximate steady-state solution is obtained in the limit of large Darcy–Rayleigh number for the quadratic profile (29) by using an asymptotic

method to investigate the flow in a horizontal boundary layer near the upper surface of the cavity. Although an exact solution of the horizontal boundary-layer equations is found, it will be shown that it can only be regarded as an approximation to the leading-order behaviour of the flow and temperature fields that emerge in the limit as $R \to \infty$. This is because it fails to take full account of the flow near the cold end of the cavity and is further discussed in Section 6.

Assuming the existence of a layer near the upper surface where $\partial/\partial z \gg \partial/\partial x$, a balance of the dominant terms in (2) and (3) as $R \to \infty$ requires that $\psi/z^2 \sim RT/x$ and $T/z^2 \sim T\psi/xz$. Since T and x are of order one within the layer it follows that ψ and z must scale with $R^{1/3}$ and $R^{-1/3}$, respectively. This is consistent with the numerical calculations of the maximum stream function value shown in Table 1. Thus, setting $z = 1 - R^{-1/3}\bar{z}$, a steady-state solution is sought in the form

$$T(x,z) = \overline{T}(x,\bar{z}) + \cdots,$$
$$\psi(x,z) = R^{1/3}\bar{\psi}(x,\bar{z}) + \cdots \tag{34}$$

as $R \to \infty$ and it follows from (2) and (3) that $\overline{T}$ and $\bar{\psi}$ satisfy the horizontal boundary-layer equations

$$\frac{\partial^2\bar{\psi}}{\partial\bar{z}^2} = -\frac{\partial\overline{T}}{\partial x}, \quad \frac{\partial^2\overline{T}}{\partial\bar{z}^2} = \frac{\partial\bar{\psi}}{\partial x}\frac{\partial\overline{T}}{\partial\bar{z}} - \frac{\partial\bar{\psi}}{\partial\bar{z}}\frac{\partial\overline{T}}{\partial x}. \tag{35}$$

Boundary conditions for $\bar{\psi}$ and $\overline{T}$ at the upper surface are

$$\bar{\psi} = 0, \quad \overline{T} = 1 - \left(1 - \frac{x}{L}\right)^2 \quad \text{on } \bar{z} = 0 \tag{36}$$

and at the lower edge of the layer it will be assumed that

$$\frac{\partial\bar{\psi}}{\partial\bar{z}} \to 0, \quad \frac{\partial\overline{T}}{\partial\bar{z}} \to 0 \quad \text{as } \bar{z} \to \infty. \tag{37}$$

Because of the quadratic profile in (36), an exact solution of these equations and boundary conditions can be found in the form

$$\bar{\psi} = L^{1/3}\left(1 - \frac{x}{L}\right)\phi_0(Z),$$
$$\overline{T} = \theta_1(Z) - \left(1 - \frac{x}{L}\right)^2\theta_0(Z), \tag{38}$$

where $\bar{z} = L^{2/3}Z$ and the functions ϕ_0, θ_0 and θ_1 satisfy the equations

$$\phi_0'' = -2\theta_0, \quad \theta_0'' - 2\phi_0'\theta_0 + \phi_0\theta_0' = 0, \quad \theta_1'' = -\phi_0\theta_1' \tag{39}$$

with boundary conditions

$$\phi_0 = 0, \quad \theta_0 = 1, \quad \theta_1 = 1 \quad \text{on } Z = 0 \tag{40}$$

and

$$\phi_0', \theta_0', \theta_1' \to 0 \quad \text{as } Z \to \infty. \tag{41}$$

Note that the solution (38) is consistent with the end conditions $\bar{\psi} = \partial\overline{T}/\partial x = 0$ at $x = L$ but does not satisfy the equivalent boundary conditions at $x = 0$; the existence of a vertical boundary layer near $x = 0$ is discussed in Section 6.

The system (39)–(41) is independent of the aspect ratio L and its solution can be found as follows. Elimination of θ_0 yields a single fourth-order equation for ϕ_0 which upon integration and use of the fact that $\phi_0 = o(Z)$ as $Z \to \infty$ gives

$$\phi_0''' + \phi_0\phi_0'' - \frac{3}{2}\phi_0'^2 = 0, \tag{42}$$

to be solved subject to

$$\phi_0 = 0, \quad \phi_0'' = -2 \quad \text{on } Z = 0, \quad \phi_0' \to 0 \quad \text{as } Z \to \infty. \tag{43}$$

At the edge of the layer ϕ_0 has the behaviour

$$\phi_0 \sim a - k\mathrm{e}^{-aZ} \quad \text{as } Z \to \infty, \tag{44}$$

where a and k are constants to be determined. These are effectively fixed by satisfying the two boundary conditions at $Z = 0$. If the asymptotic solution (44) were valid for all Z it would follow that $k = a = 2^{1/3}$ and the actual solution of (42) and (43) was found by using this as an initial guess in a Newton iteration. A fourth-order Runge–Kutta scheme was used to integrate (42) inwards from the form (44) at a suitable outer boundary $Z = Z_\infty$ and then the Newton iteration used to home in on the zeros of $\phi_0(0)$ and $\phi_0''(0) + 2$. The constants a and k converged to the final values

$$a = 1.141, \quad k = 1.021 \tag{45}$$

and the first derivative of ϕ_0 at the origin was found to be

$$c = \phi_0'(0) = 1.447. \tag{46}$$

Graphs of ϕ_0 and ϕ_0' are shown in Fig. 10, along with θ_0 which can now be found from the relation $\theta_0 = -\frac{1}{2}\phi_0''$. Note that $\theta_0 \to 0$ as $Z \to \infty$.

Finally, θ_1' is found by integrating the third equation in (39) to give

$$\theta_1' = -A\exp\left(-\int_0^Z \phi_0\,\mathrm{d}Z\right), \tag{47}$$

where A is an arbitrary constant. One further integration then gives

$$\theta_1 = 1 - A\Theta_1, \tag{48}$$

where

$$\Theta_1 = \int_0^Z \exp\left(-\int_0^Z \phi_0(Z')\,\mathrm{d}Z'\right)\mathrm{d}Z \tag{49}$$

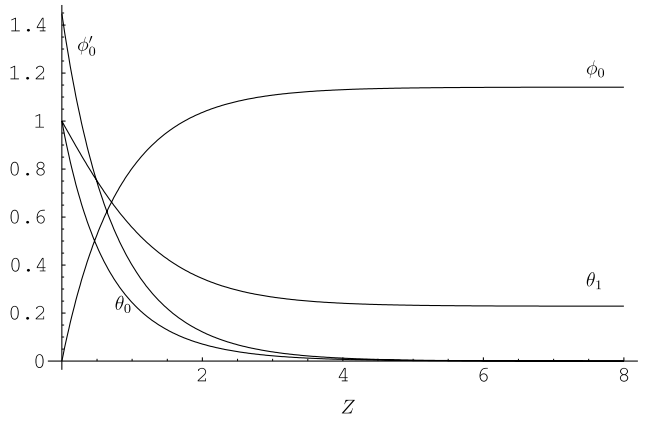

Fig. 10. The horizontal boundary-layer functions ϕ_0, ϕ_0', θ_0 and θ_1.

and it follows that

$$\theta_1 \to 1 - A\chi_0 \quad \text{as } Z \to \infty, \tag{50}$$

where

$$\chi_0 = \int_0^\infty \exp\left(-\int_0^Z \phi_0(Z')\,\mathrm{d}Z'\right)\mathrm{d}Z = 1.472. \tag{51}$$

In order to find the constant A and thus complete the horizontal boundary-layer solution, it is noted that, for the overall steady-state solution in the cavity, the heat flux Q at the upper boundary (defined by (28)) must vanish. In the limit as $R \to \infty$ the dominant contribution to this integral must come from the horizontal boundary-layer region, and so it follows that

$$\int_0^L \frac{\partial \overline{T}}{\partial \bar{z}}(x,0)\,\mathrm{d}x = 0. \tag{52}$$

Substituting for $\overline{T}$ from (38) and performing the integration in x gives

$$\theta_1'(0) - \frac{1}{3}\theta_0'(0) = 0 \tag{53}$$

and since $\theta_1'(0) = -A$ and

$$\theta_0'(0) = -\frac{1}{2}\phi_0'''(0) = -\frac{3}{4}(\phi_0'(0))^2 = -\frac{3}{4}c^2, \tag{54}$$

it follows that

$$A = \frac{1}{4}c^2 = 0.524. \tag{55}$$

This completes the solution for θ_1, which is shown in Fig. 10. It is seen that

$$\theta_1 \to b = 1 - \frac{1}{4}c^2\chi_0 = 0.229 \quad \text{as } Z \to \infty. \tag{56}$$

This predicts a temperature in the cavity below the horizontal layer which is constant and given to leading order as $R \to \infty$ by

$$T(x,z) \sim b = 0.229, \tag{57}$$

a result which is in reasonable accord with the numerical findings of Section 4.

The overall temperature profile at the end $x = 0$ of the horizontal boundary layer is given by

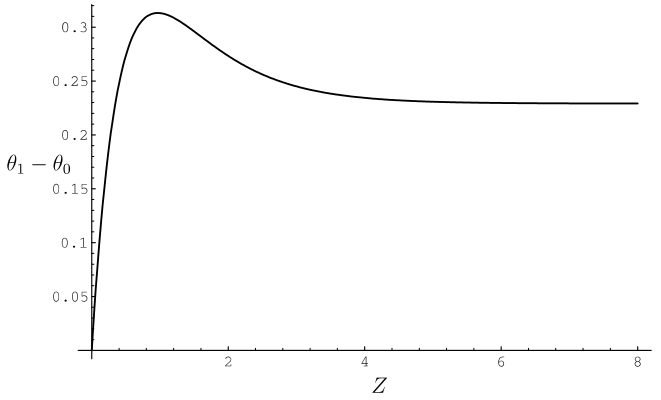

Fig. 11. The temperature profile $\theta_1 - \theta_0$ at the end of the horizontal boundary layer.

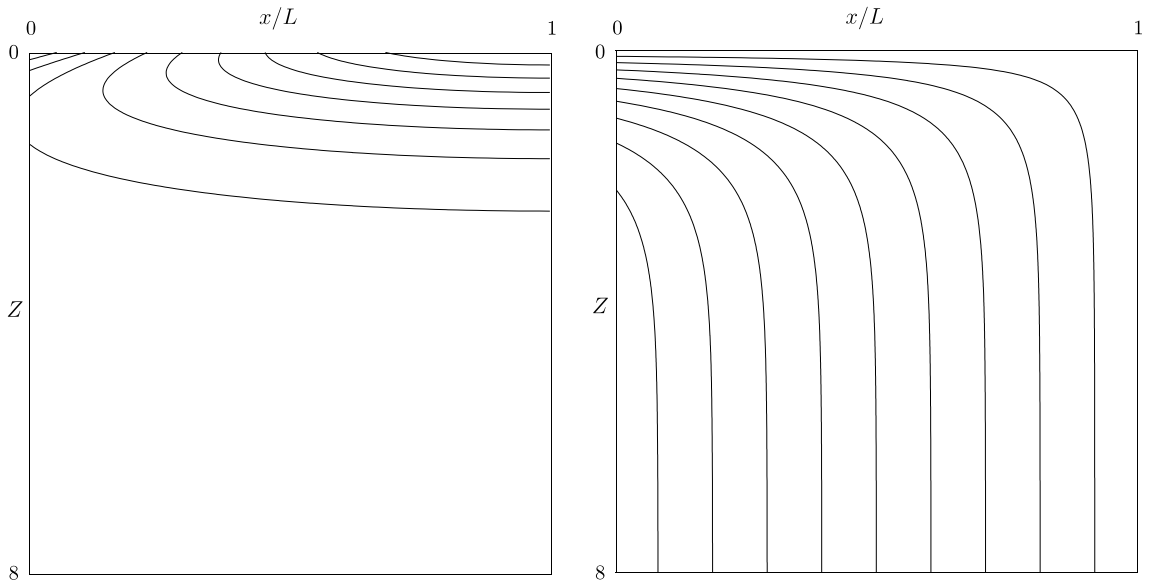

Fig. 12. Isotherms and streamlines of the horizontal boundary-layer solution.

$$\overline{T}(0,\bar{z}) = \theta_1(Z) - \theta_0(Z) \tag{58}$$

and is shown in Fig. 11. It reaches a maximum value of $\overline{T} = 0.313$ at $\bar{z} = \bar{z}_0 = L^{2/3}Z_0 = 0.96L^{2/3}$ and then decreases to the asymptotic value $\overline{T} \sim 0.229$ as $\bar{z} \to \infty$. The corresponding stream function profile at $x = 0$ is

$$\bar{\psi}(0,\bar{z}) = L^{1/3}\phi_0(Z) \tag{59}$$

and reaches a maximum value of $\bar{\psi} \sim 1.141L^{1/3}$ as $\bar{z} \to \infty$. The corresponding scaled horizontal velocity $\bar{u}(0,\bar{z}) = -L^{-1/3}\phi_0'$, where ϕ_0' is shown in Fig. 10, is in the negative x direction and feeds fluid entrained by the horizontal layer into the cold corner. This inflow is maximum at the upper surface and reduces to zero at the bottom of the horizontal layer. Streamlines and isotherms of the horizontal boundary-layer solution are shown in Fig. 12.

6. Discussion

Numerical and asymptotic solutions for cavity flow in a porous medium driven by differential heating of the upper surface have been found for a range of Darcy–Rayleigh numbers. For a monotonic temperature distribution at the upper surface and thermally insulated lower walls, a single-cell circulation is generated, the centre of which moves to the upper cold corner of the cavity as the Darcy–Rayleigh number increases. The general features of the limiting structure as $R \to \infty$ have been confirmed by a boundary-layer analysis. In particular, the temperature distribution in the horizontal boundary layer at the upper surface and the predicted core temperature (57) are remarkably consistent with the numerical calculations of Section 4. The streamlines of the horizontal boundary-layer solution (Fig. 12) indicate a flow drawn into the lower edge of the layer and then conveyed to the cold end where it is expelled from the layer. Here the comparison with the numerical calculations is less convincing, both in terms of the implied existence of a region of predominantly upward velocity below the thermal variation in the layer (not seen in the numerical calculations) and the non-existence of a closed eddy at the end of the layer (seen in the numerical calculations). The reason for the discrepancy is now discussed.

The exact solution of the horizontal boundary-layer equations found here imposes both a horizontal velocity and a temperature profile at the end $x = 0$ of the layer which must be adjusted in order to achieve the boundary conditions $\psi = \partial T/\partial x = 0$ on the sidewall of the cavity. The vertical boundary layer needed to achieve this adjustment occupies a narrow region with lateral scale $x \sim R^{-2/3}$ near the sidewall. The exponential decay of the solution there to the horizontal boundary-layer profiles $T_\infty(\bar{z}) = \overline{T}(0,\bar{z})$ and $\psi_\infty(\bar{z}) = \bar{\psi}(0,\bar{z})$ is given by the real part of

$$\exp(-\lambda(\bar{z})R^{2/3}x), \tag{60}$$

where

$$\lambda = \lambda_\pm = \frac{\psi_\infty \pm (\psi_\infty'^2 - 4T_\infty')^{1/2}}{2} \tag{61}$$

(see, for example, [11]) and the real part of λ must be positive. For the horizontal boundary-layer profiles (58) and (59), $\psi'_\infty > 0$ and $T'_\infty > 0$ when $\bar{z} < \bar{z}_0$ so that both roots (61) have positive real part (real if $\psi'^2_\infty > 4T'_\infty$ and complex conjugates if $\psi'^2_\infty < 4T'_\infty$). Thus it is possible that *both* $\psi_\infty(\bar{z})$ and $T_\infty(\bar{z})$ can be specified when solving the vertical boundary-layer equations in this region.

For $\bar{z} > \bar{z}_0$, however, $\psi'_\infty > 0$ and $T'_\infty < 0$ so that λ_+ is positive and λ_- is negative. Thus it can be expected that at most one of the edge profiles $\psi_\infty(\bar{z})$ and $T_\infty(\bar{z})$ can be specified when solving the vertical boundary-layer equations in this region. For this reason, the horizontal boundary-layer solution obtained in Section 5 cannot be the correct one, as it determines both ψ_∞ and T_∞ in the region $\bar{z} > \bar{z}_0$. The resolution of this difficulty requires a detailed study of the combined horizontal/vertical boundary-layer systems and is considered in a separate paper [31]. Nevertheless the approximate theory presented here provides an excellent approximation to both the velocity and temperature fields in the upper section of the horizontal boundary layer ($\bar{z} < \bar{z}_0$) and to the core temperature.

Finally, it is worth mentioning some extensions and applications of the present analysis. First, it is evident through the transformation $T \to 1 - T$, $z \to 1 - z$ and $\psi \to -\psi$ that the solutions obtained here also apply to a cavity whose upper surfaces are thermally insulated and whose *lower* surface is subject to a temperature differential $T = 1 - S(x/L)$. In this case the solution at high Darcy–Rayleigh numbers is seen to consist of an eddying motion centred on the lower hot corner, with fluid rising in a narrow vertical jet locally. The asymmetry of the flow field may be relevant to understanding why relatively small regions of hot upwelling are observed in many geothermal fields. Another extension of the present work is to the case where the temperature profile $S(x/L)$ is non-monotonic. For example, a profile of the form (9) applied to the upper surface of an enlarged cavity $-L \leqslant x \leqslant L$, $0 \leqslant z \leqslant 1$ (representing a temperature differential with a minimum at the centre, $x = 0$) would generate a double-cell circulation formed by exactly the same streamlines and isotherms in the region $0 \leqslant x \leqslant L$ together with their reflections about $x = 0$ in the region $-L \leqslant x \leqslant 0$. This is because the centreline $x = 0$, $0 \leqslant z \leqslant 1$ of the enlarged cavity is a line of symmetry on which $\psi = \partial T/\partial x = \partial w/\partial x = 0$, and is therefore consistent with the boundary conditions (6) applied at $x = 0$.

Acknowledgements

One of us (MP) is grateful for financial support from the Ministry of University Affairs in Thailand. The authors also thank Ms P. Adamou-Graham for assistance.

References

[1] E.R. Lapwood, Convection of a fluid in a porous medium, Proc. Camb. Philos. Soc. 44 (1948) 508.
[2] B.K.C. Chan, C.M. Ivey, J.M. Barry, Natural convection in enclosed porous media with rectangular boundaries, J. Heat Transfer 92 (1970) 21.
[3] C.E. Hickox, D.K. Gartling, A numerical study of natural convection in a horizontal porous layer subjected to an end-to-end temperature difference, J. Heat Transfer 103 (1981) 797.
[4] V. Prasad, F.A. Kulacki, Convective heat transfer in a rectangular porous cavity—effect of aspect ratio on flow structure and heat transfer, J. Heat Transfer 106 (1984) 158.
[5] S. Klarsfeld, Champs de temperature associes aux movements de convection naturelle dans un milieu poreux limite, Rev. Gen. Therm. 9 (1970) 1403.
[6] C.G. Bankvall, Natural convection in a vertical permeable space, Warme Stoffubertr. 7 (1974) 22.
[7] M.A. Combarnous, S.A. Bories, Hydrothermal convection in saturated porous media, Adv. Hydrosci. 10 (1975) 232.
[8] N. Seki, S. Fukusako, H. Inaba, Heat transfer in a confined rectangular porous cavity packed with porous media, Int. J. Heat Mass Transfer 21 (1978) 985.
[9] J.E. Weber, The boundary-layer regime for convection in a porous cavity, Int. J. Heat Mass Transfer 18 (1975) 569.
[10] K. Walker, G.M. Homsy, Convection in a porous cavity, J. Fluid Mech. 87 (1978) 449.
[11] P.A. Blythe, P.G. Daniels, P.G. Simpkins, Thermally driven cavity flows in porous media I. The vertical boundary-layer structure near the corners, Proc. R. Soc. London A380 (1982) 119.
[12] P.G. Daniels, P.A. Blythe, P.G. Simpkins, Thermally driven cavity flows in porous media II. The horizontal boundary-layer structure, Proc. R. Soc. London A382 (1982) 135.
[13] P.G. Daniels, P.A. Blythe, P.G. Simpkins, Thermally driven shallow cavity flows in porous media: the intermediate regime, Proc. R. Soc. London A406 (1986) 263.
[14] P.G. Daniels, P.A. Blythe, P.G. Simpkins, Thermally driven cavity flows in porous media: the merged layer regime, Proc. R. Soc. London A426 (1989) 107.
[15] A. Ansari, P.G. Daniels, Thermally driven tall cavity flows in porous media, Proc. R. Soc. London A433 (1993) 163.
[16] A. Ansari, P.G. Daniels, Thermally driven tall cavity flows in porous media: the convective regime, Proc. R. Soc. London A444 (1994) 375.
[17] P. Cheng, I.D. Chang, On buoyancy induced flows in a saturated porous medium adjacent to impermeable horizontal surfaces, Int. J. Heat Mass Transfer 19 (1976) 1267.
[18] I.D. Chang, P. Cheng, Matched asymptotic expansions for free convection about an impermeable horizontal surface in a porous medium, Int. J. Heat Mass Transfer 26 (1983) 163.
[19] D.A.S. Rees, A.P. Bassom, The nonlinear non-parallel wave instability of boundary-layer flow induced by a horizontal heated surface in porous media, J. Fluid Mech. 253 (1993) 267.
[20] D.A.S. Rees, A.P. Bassom, The linear wave instability of boundary-layer flow induced by a horizontal heated

surface in porous media, Int. Commun. Heat Mass Transfer 21 (1994) 143.
[21] P. Cheng, W.J. Minkowycz, Free convection about a vertical flat plate embedded in a porous medium with application to heat transfer from a dike, J. Geophys. Res. 82 (1977) 2040.
[22] J.H. Merkin, Mixed convection boundary-layer flow on a vertical surface in a saturated porous medium, J. Eng. Math. 14 (1980) 301.
[23] D.B. Ingham, J.H. Merkin, I. Pop, Flow past a suddenly cooled vertical flat surface in a saturated porous medium, Int. J. Heat Mass Transfer 25 (1982) 1916.
[24] V. Joshi, B. Gebhart, Vertical natural convection flows in porous media: calculations of improved accuracy, Int. J. Heat Mass Transfer 27 (1984) 69.
[25] D.B. Ingham, S.N. Brown, Flow past a suddenly heated vertical plate in a porous medium, Proc. R. Soc. London A403 (1986) 51.
[26] P.G. Daniels, P.G. Simpkins, The flow induced by a heated vertical wall in a porous medium, Quart. J. Mech. Appl. Math. 37 (1984) 339.
[27] D.B. Ingham, I. Pop, Free convection from a semi-infinite vertical surface bounded by a horizontal wall in a porous medium, Int. J. Heat Mass Transfer 30 (1987) 1615.
[28] D.A.S. Rees, A.P. Bassom, Some exact solutions for free convection flows over heated semi-infinite surfaces in porous media, Int. J. Heat Mass Transfer 34 (1991) 1564.
[29] D.A. Nield, A. Bejan, Convection in Porous Media, Springer-Verlag, Berlin, 1999.
[30] J. Chery, A. Bonneville, P.J. Vilotte, D. Yuen, Numerical modelling of caldera dynamical behaviour, Geophys. J. Int. 105 (1991) 365.
[31] P.G. Daniels, M. Punpocha, On the boundary-layer structure of cavity flow in a porous medium driven by differential heating, J. Fluid Mech. (submitted).